Flutter control of a flat plate section model using nonlinear vibration absorbers

Alexandre Pécheux, Xavier Amandolese, A Malher, Pascal Hémon, Cyrille Stephan

FLUTTER CONTROL OF A FLAT PLATE SECTION MODEL USING NONLINEAR VIBRATION ABSORBERS

A. Pécheux[1], X. Amandolese[2], A. Malher[3], P. Hémon[3], C. Stephan[1]

[1]ONERA, The French Aerospace Lab, DAAA/MSAE, Châtillon, France
alexandre.pecheux@onera.fr

[2]LMSSC, Conservatoire National des Arts et Métiers, Paris, France
xavier.amandolese@lecnam.net

[3]LadHyX, Ecole Polytechnique, Palaiseau, France

Keywords: Flutter, control, aeroelasticity, wind tunnel, dynamic stall model

Abstract: The present work focuses on flutter mitigation of a flat plate section model using passive linear and nonlinear vibration absorbers for a two branches (coupled-mode flutter and stall flutter) post-critical flutter scenario. Experiments have been done in a subsonic wind tunnel using an aeroelastic section model set-up. Numerical results have been obtained using an analytical section model for which the pitch-plunge-absorbers equations of motion are combined with a nonlinear unsteady aerodynamic formulation. Without control, the two branches post-critical flutter scenario is well captured by the numerical model. Using linear or non linear vibrations absorbers in plunge, qualitative agreement are found. Adding a non linear absorber in pitch, numerical prediction does not match the one obtained in wind tunnel. This study however confirms that a combination of absorbers in both pitch and plunge is the best solution to delay the critical velocity and that a proper numerical tuning should also help to optimize the LCOs mitigations.

1 INTRODUCTION

The "bending-torsion" flutter of lifting surfaces, often called coupled-mode flutter, is a dynamic instability for which self-sustained oscillations occur above a critical speed. This flutter relies on fluid-elastic coupling where combined plunging and pitching motions can produce interactions and phase shifts in a way that energy is transferred from the flow to the structure [1]. The stall flutter is a dynamic instability that does not depend on coupling. This phenomenon is of particular importance for wings or blades operating at high angles of attack. In such cases, torsion is the mode of vibration the most commonly involved. The mechanism for energy transfer then relies on a dynamic stall process for which the flow separates partially or completely during each cycle of oscillation. Numerous investigations on the coupled-mode flutter or stall flutter post-critical behaviors can be found. Most of these studies focus on the impact of nonlinearities encountered in aeronautics (see [2–4], for a review). Experimental evidence of post-critical LCOs using an aeroelastic "pitch-plunge" section model set-up has also been reported in [5] and [6]. In the later, two LCO branches associated to nonlinear aerodynamics saturation have been found in the post-critical regime. The first one being reached increasing the velocity beyond the coupled-mode flutter critical velocity and the second one occurring when the LCO amplitude in pitch enters the stall region. This second LCO branch was then reported as a symmetric stall flutter regime.

Flutter control is an important research topic in aeronautics. In the last decades, the most explored strategy to prevent flutter was based on active control using aerodynamic surfaces. Passive control strategies using discrete devices have also been investigated. Lee and co-workers focussed on a nonlinear energy sink (NES) device [7, 8] and the concept of nonlinear tuned vibration absorbers (NLTVA) was investigated in [9–11]. Most of these studies have been performed on a wing flutter scenario for which the LCOs were due to hardening stiffness nonlinearity.

The present work focuses on flutter mitigation using passive linear and nonlinear vibration absorbers for a two branches post-critical flutter scenario highlighted in [6]. Experiments have been done in a subsonic wind tunnel using a dedicated aeroelastic section model set-up. Numerical results have been obtained using a theoretical section model for which the pitch-plunge-absorbers equations of motion are combined with a nonlinear unsteady aerodynamic formulation based upon the ONERA semi-empirical dynamic stall model [12].

The paper is organized as follows: the experimental set-up is presented in section 2. The theoretical model including the ONERA dynamic stall formulation are introduced in section 3. Bifurcation diagram in the post-critical regime are reported in section 4 for the reference configuration (without absorbers) and four different configurations of control: using a linear TMD in plunge, a NLTVA in plunge, a NLTVA in pitch and NLTVAs in both plunge and pitch.

2 EXPERIMENTAL SETUP

The experiments were performed in a subsonic closed-loop wind tunnel at LadHyX which has a rectangular test section of 0.26 m in width and 0.24 m in height. Flutter control using discrete vibrations absorbers was studied using a section model aeroelastic setup that enables high amplitude pitch-plunge motion without nonlinear structural limitations (see figure 1). The "plunge" motion is provided by two parallel shafts, mounted in four cylindrical air bearings and using a set of four linear springs. This ensures a horizontal displacement of the section model allowing the work of the absorber device without gravity impact. The axis of rotation was linked to both the horizontal shafts by two bearings and the rotational stiffness was set by two spiral torsion springs. The setup allows to change both the position of the section model centre of rotation and gravity center.

In the present study we will focus on the mitigation of post-critical behaviors observed for a a rigid flat plate model of thickness-to-chord ratio 4.3% with a mean angle of attack set at zero and an elastic centre at the mid-chord. This aeroelastic configuration exhibits a two branches post-criticall flutter (i.e. from coupled-mode flutter to high amplitude symmetric stall flutter, see section 4). Two magnetic vibrations absorbers (MVAs) were used. The MVA used in plunge is inspired from the one developed by [13]. Changing the magnetic arrangement it can be tuned to a LTVA (i.e. a TMD) or a NLTVA (with cubic stiffness). The setup shown in figure 1, also shows a rotating MVA. This new concept of MVA was especially designed for testing nonlinear control strategies on pitch.

3 AEROELASTIC SECTION MODEL

The equations of motion for the pitch-plunge section model coupled with the absorbers in pitch and plunge (see figure 2) can be expressed, as following:

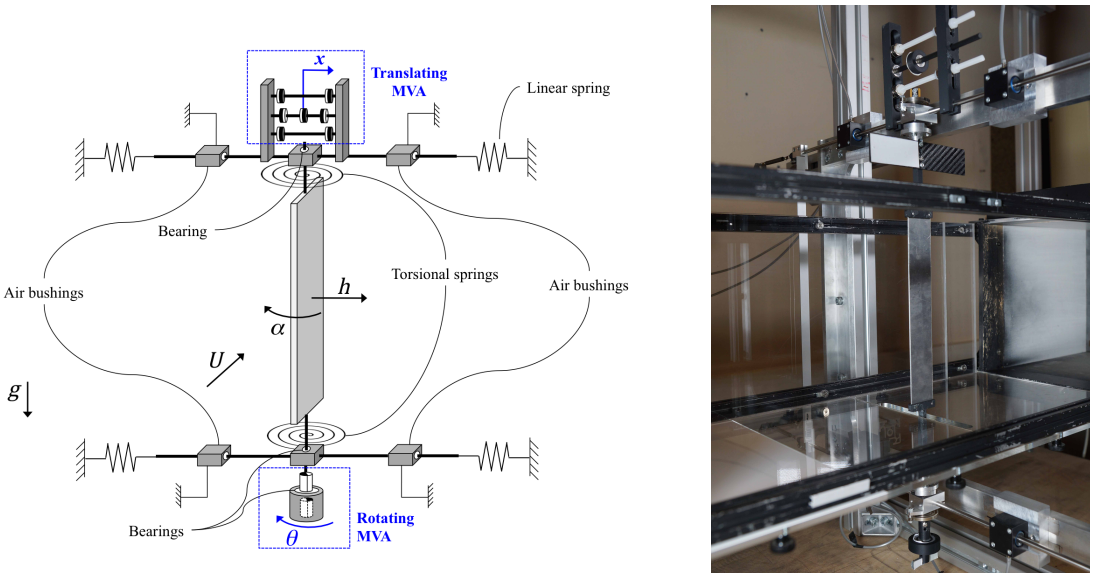

Figure 1: Pitch-plunge aeroelastic set-up used for the test of magnetic vibration absorbers; (left) schematic and (right) view of the setup in wind tunnel.

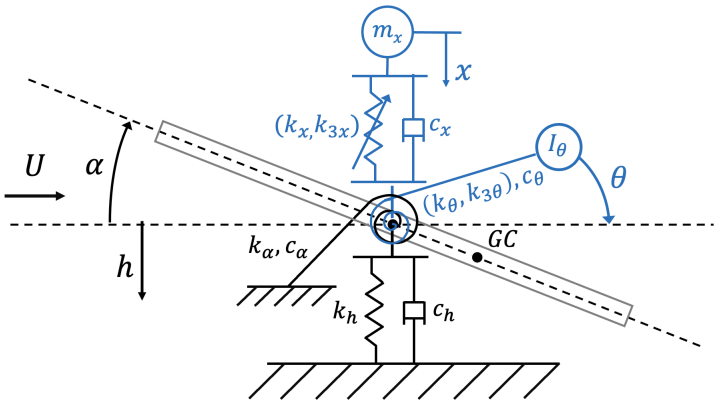

Figure 2: Sketch of the two degrees-of-freedom section model (black) coupled with the absorbers in pitch and plunge (blue).

$$
\begin{aligned}
mh'' + S_\alpha\big(\cos(\alpha)\alpha'' - \sin(\alpha)\alpha'^2\big) + c_h h' + k_h h + c_z(h' - x') + k_x(h - x)) + k_{3x}(h - x)^3 = -L,\\
I_a\alpha'' + S_a\cos(\alpha)h'' + c_\alpha\alpha' + k_\alpha\alpha + c_\theta(\alpha' - \theta') + k_\theta(\alpha - \theta) + k_{3\theta}(\alpha - \theta)^3 = M,\\
m_x x'' + c_x(x' - h') + k_x(x - h) + k_{3x}(x - h)^3 = 0,\\
I_\theta\theta'' + c_\theta(\theta' - \alpha') + k_\theta(\theta - \alpha) + k_{3\theta}(\theta - \alpha)^3 = 0,
\end{aligned}
\tag{1}
$$

where the flat plate two degrees of freedom are described by the angle of rotation α (positive nose up) and the heave h (positive downward and measured at the elastic axis), the parameters m, I_α, c_h, c_α, k_h, k_α are the primary system's mass, moment of inertia about the elastic axis, structural damping and stiffness in plunge and pitch, per unit length. $S_\alpha = mx_{GC}$ is the static moment of the flat-plate model about the elastic axis, intoducing x_{GC} the distance from the elastic centre to the centre of gravity. L and M are respectively the aerodynamic lift (positive upward) and pitching moment (positive leading-edge up) about the elastic axis, acting on the flat-plate model. In the present study both the absorbers in plunge and pitch have been connected to the elastic center (see figure 2). The absorber in plunge is described by its linear displacement

x, mass m_x, damping coefficient c_x and both linear and cubic stiffness coefficients k_x and k_{3x}. The absorber in pitch is described by its angle of rotation θ, moment of inertia I_θ, damping coefficient c_θ, linear and cubic stiffness coefficients, k_θ and $k_{3\theta}$.

The equations of motion 1 can be expressed in nondimensional form (using the reduced time defined as $\tau = \frac{Ut}{b}$), where U is the mean flow velocity and b is the semi-chord of the flat plate:

$$\begin{array}{c}
\frac{\ddot{h}}{b} + 2\eta_h k_\alpha \Omega \frac{\dot{h}}{b} + k_\alpha^2 \Omega^2 \frac{h}{b} + x_\alpha \big(\cos(\alpha)\ddot{\alpha} - \sin(\alpha)\dot{\alpha}^2 \big) \\
+2\eta_x \epsilon_x k_\alpha \Omega_x (\frac{\dot{h}}{b} - \frac{\dot{x}}{b}) + \epsilon_x k_\alpha^2 \Omega_x^2 \big((\frac{h}{b} - \frac{x}{b}) + \beta_x (\frac{h}{b} - \frac{x}{b})^3 \big) = -\frac{1}{\pi\mu} C_L, \\
\ddot{\alpha} + 2\eta_\alpha k_a \dot{\alpha} + k_\alpha^2 \alpha + \frac{x_\alpha}{r_g^2} \cos(\alpha) \frac{\ddot{h}}{b} \\
+2\eta_\theta \epsilon_\theta k_\alpha \Omega_\theta (\dot{\alpha} - \dot{\theta}) + \epsilon_\theta k_\alpha^2 \Omega_\theta^2 \big((\alpha - \theta) - \beta_\theta (\alpha - \theta)^3 \big) = \frac{2}{\pi \mu r_g^2} C_M, \\
\frac{\ddot{x}}{b} + 2\eta_x k_\alpha \Omega_x (\frac{\dot{x}}{b} - \frac{\ddot{h}}{b}) + k_\alpha^2 \Omega_x^2 \big((\frac{x}{b} - \frac{h}{b}) + \beta_x (\frac{x}{b} - \frac{h}{b})^3 \big) = 0, \\
\ddot{\theta} + 2\eta_\theta k_\alpha \Omega_\theta (\dot{\theta} - \dot{\alpha}) + k_\alpha^2 \Omega_\theta^2 \big((\theta - \alpha) + \beta_\theta (\theta - \alpha)^3 \big) = 0,
\end{array} \tag{2}$$

where dimensionless parameters for the primary system (i.e. the 2dof section model) are : the plunge to pitch natural frequencies ratio $\Omega = \frac{\omega_h}{\omega_\alpha}$, the damping ratios in plunge and pitch η_h and η_α, the reduced frequency based on the pitch natural frequency $k_\alpha = \frac{b\omega_\alpha}{U}$, the non-dimensional radius of gyration about its elastic centre $r_g = \sqrt{\frac{I_\alpha}{mb^2}}$, the solid/fluid mass ratio $\mu = \frac{m}{\pi \rho b^2}$, the distance in semi-chord from the elastic centre to the centre of gravity $x_\alpha = \frac{x_{GC}}{b}$, the aerodynamic lift coefficient and pitching moment coefficient about the elastic axis $C_L = \frac{L}{\rho U^2 b}$ and $C_M = \frac{M}{2\rho U^2 b^2}$.

Regarding the absorbers, the nondimensional parameters are the damping ratios $\eta_x = \frac{c_x}{2\sqrt{k_x m_x}}$ and $\eta_\theta = \frac{c_\theta}{2\sqrt{k_\theta I_\theta}}$, the mass and inertia ratio $\varepsilon_x = \frac{m_x}{m}$ and $\varepsilon_\theta = \frac{I_\theta}{I_\alpha}$, the absorber to pitch natural frequencies ratio $\Omega_x = \frac{\omega_x}{\omega_\alpha}$ and $\Omega_\theta = \frac{\omega_\theta}{\omega_\alpha}$, the nondimensional cubic nonlinear stiffness factor $\beta_x = \frac{k_{3x}}{k_x} b^2$ and $\beta_\theta = \frac{k_{3\theta}}{k_\theta}$

3.1 Dynamic stall model

The ONERA dynamic stall model has been used for the unsteady lift and moment calculation. It is a semi-empirical model introduced in [12] and improved in [14] that allows to reproduce the nonlinear dynamic response in both lift and moment due to dynamic stall processes. To take into account both the effect of pitch and plunge, two effective angles of attack are introduced: $\theta_0 = \alpha - \frac{\dot{h}}{b}$ which is the effective angle of attack at the elastic center and $\theta_1 = \frac{\dot{\alpha}}{2}$ which is a pitch rate (or induced camber) contribution. Note that $\theta_0 + \theta_1$ defines an effective angle of attack at the 3/4 chord location. In the following the model is written in reduced time $\tau = \frac{tU}{b}$:

$$\begin{array}{c}
C_{L_d} = \pi \dot{\theta}_0 + \frac{\pi}{2} \dot{\theta}_1 + C_{L1} + C_{L2}, \\
\dot{C}_{L1} + \lambda C_{L1} = \lambda \frac{dC_L}{d\alpha} \theta_0 + \lambda \sigma_{s,L} \theta_1 + \left[\beta \frac{dC_L}{d\alpha} + \sigma_{1,L} \left| \Delta C_L \left(\theta_0 \right) \right| \right] \dot{\theta}_0 + \beta \sigma_{s,L} \dot{\theta}_1, \\
\ddot{C}_{L2} + c_{a,L} \dot{C}_{L2} + c_{r,L} C_{L2} = -c_{r,L} \Delta C_L \left(\theta_0 \right) - c_{e,L} \dot{\theta}_0.
\end{array} \tag{3}$$

$$\begin{array}{c}
C_{M_d} = C_{M1} + C_{M2}, \\
C_{M1} = \frac{dC_M}{d\alpha} \theta_0 + \sigma_p \theta_1 + \left(\sigma_b + \sigma_{1,M} \left| \Delta C_L \left(\theta_0 \right) \right| \right) \dot{\theta}_0 + \sigma_{s,M} \dot{\theta}_1, \\
\ddot{C}_{M2} + c_{a,M} \dot{C}_{M2} + c_{r,M} C_{M2} = -c_{r,M} \Delta C_M \left(\theta_0 \right) - c_{e,M} \dot{\theta}_0.
\end{array} \tag{4}$$

where $\frac{dC_L}{d\alpha}$ and $\frac{dM_L}{d\alpha}$ are the slopes of the lift and moment steady coefficient at small angle of attack (linear region). $\Delta C_L(\theta_0)$ and $\Delta C_M(\theta_0)$ quantify the degree of separation for both lift and moment (difference between the linear lift or moment coefficient from an extrapolation of the linear region and the static lift or moment coefficient for the effective angle of attack θ_0.) For the unstalled contribution in lift and moment eigth parameters are needed $\lambda, \sigma_{s,L}, \beta$ and $\sigma_{1,L}$ for C_{L1} and $\sigma_p, \sigma_b, \sigma_{s,M}$ and $\sigma_{1,M}$ for C_{M1}. For both the lift and moment the dynamic response in the non linear stalled region is the solution of a second order oscillatory equation with a forcing that depends on both the degree of separation (the nonlinear deviation ΔC_L or ΔC_M) and pitch rate. Three additional parameters are required c_a, c_r, c_e that also depend on the degree of separation in lift: $c_r = \left(r_0 + r_2 \left(\Delta C_L\right)^2\right)^2, c_a = a_0 + a_2 \left(\Delta C_L\right)^2, c_e = e_2 \left(\Delta C_L\right)^2$. Recommended values for r_0, r_2, a_0, a_2, e_2 differ between the lift and moment. In the present study they have been identified using dynamics tests in forced pitching motion. Following the recommendation of Petot [14] which was inspired from the work of Beddoes [15], a time delay can also be used to take into account a dynamic stall delay. It consists of setting $\Delta C_L = 0$ for a reduced time $\Delta\tau_L$ after the airfoil pitch up threw the static stall angle of attack. The same procedure can be applied for the nonlinear deviation of the moment ΔC_M.

A static and dynamic loop database obtained previously for a flat plate section model of the same thickness-to-chord ratio, in the same wind tunnel and for the same range of Reynolds number ($Re \approx 40000$), was used to identified the parameters of the model reported in tables 1 and 2. Unsteady lift and moment measured for forced harmonic symmetric pitch motions have also shown that $\Delta\tau_L$ and $\Delta\tau_M$ are function of the amplitude and reduced pulsation. In the present study the following empirical laws have been used : $\Delta\tau_L = 11 - 85\tilde{\theta}_0 k$ and $\Delta\tau_M = 8 - 100\tilde{\theta}_0 k$, where $k = \frac{b\omega}{U}$ is the reduced pulsation and $\tilde{\theta}_0$ is the amplitude of the effective angle of attack. Note that during the recovery process, the degree of separation ΔC_L and ΔC_M, in both lift and moment, need also to be reduced with a coefficient that was found to follow: $c_\Delta = (|\theta_0|/\tilde{\theta}_0)^{k/0.06}$.

A validation of the ONERA dynamic stall model (and parameters) for a flat plate section in forced symmetric pitching motion of reduced frequency $k = 0.06$, Reynolds number $Re = 40000$ and three amplitude $\tilde{\alpha} = 12°$, $27°$ and $45°$ is shown in figure 3.

Table 1: Dynamic stall parameters for the lift

λ	$\sigma_{s,L}$	$\sigma_{1,L}$	β	$r_{0,L}$	$r_{2,L}$	$a_{0,L}$	$a_{2,L}$	$e_{2,L}$
0.17	2π	-0.04	0.53	0.3	0.05	0.79	0.2	-0.1

Table 2: Dynamic stall parameters for the moment

$\sigma_{s,M}$	$\sigma_{1,M}$	σ_p	σ_b	$r_{0,M}$	$r_{2,M}$	$a_{0,M}$	$a_{2,M}$	$e_{2,M}$
$-3\pi/16$	0	$-3\pi/16$	$-5\pi/16$	0.32	0.05	0.56	0.1	-0.1

4 RESULTS

Flutter mitigation using passive linear and nonlinear vibration absorbers has been studied for a two branches post-critical flutter scenario observed in wind tunnel with the aeroelastic parameters reported in table 3.

Bifuraction diagrams measured in wind tunnel are reported in figure 4 (in black). One can observe a post-critical behavior with two LCO branches: a coupled-mode flutter branch with low amplitude in pitch and moderate amplitude in plunge, a symmetric stall flutter branch with high

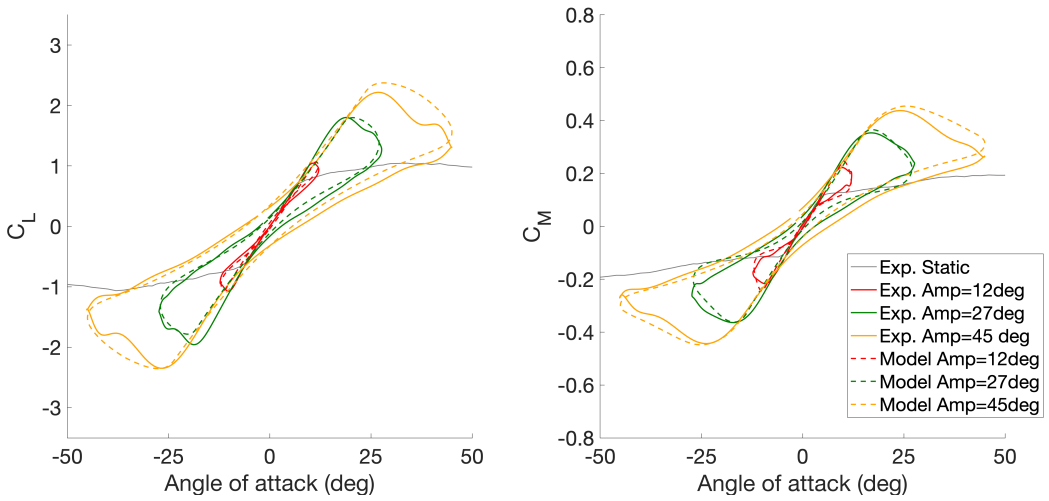

Figure 3: Validation of the ONERA dynamic stall model for a flat plate section model at Reynolds number $Re = 40000$ in forced symmetric pitching motion of reduced frequency $k = 0.06$ for amplitude $\tilde{\alpha} = 12°$, $27°$ and $45°$. Solid line (experiment), dashed line (model). Steady curves (experiment) are reported in grey line.

Table 3: Non-dimensional aeroelastic parameters

$\Omega = \frac{\omega_h}{\omega_\alpha}$	r_g	μ	η_h	η_α	x_α
0.778	0.658	3307	0.015	0.005	0.033

amplitude in pitch and low amplitude in plunge, along with a hysteretic behavior decreasing the velocity from the stall flutter branch. The amplitude of limit cycle oscillations in both pitch and plunge obtained with the theoretical model are also reported in figure 4 (in red). The model also exhibits a two branches post-critical flutter scenario. One can however notice that the critical velocity is slightly overestimated, reducing the range of the coupled-mode flutter branch. Regarding the stall flutter branch, the amplitude LCOs in pitch are also underestimated while they are overestimated in plunge. Anyway the qualitative behavior is quite good.

Four different configurations of vibrations absorbers have been tested in wind tunnel : a linear TMD in plunge, a NLTVA in plunge, a NLTVA in pitch and NLTVAs in both plunge and pitch. Associated nondimensional parameters are reported in table 4.

Table 4: TMD and NLTVA nondimensional parameters

	$\varepsilon_{x,\theta}$	$\Omega_{x,\theta}$	$\eta_{x,\theta}$	$\beta_{x,\theta}$
TMD-Plunge	0.01	0.866	≈ 0.01	0
NLTVA-Plunge	0.012	0.8325	≈ 0.01	2.1
NLTVA-Pitch	0.025	0.75	≈ 0.01	0.2

Bifuraction diagrams measured for each configuration are reported in figure 5 (up). As expected, the TMD in plunge satisfactorily delays the critical velocity but the system immediately branches to the stall flutter regime, with amplitude slightly higher than the one observed without control. The NLTVA in plunge has also a beneficial impact on the critical flutter velocity and also decreases the LCO in plunge (of almost 10%), while mitigating the hysteresis effect. The NLTVA in pitch has no impact on flutter velocity but it greatly delays the switch to the stall

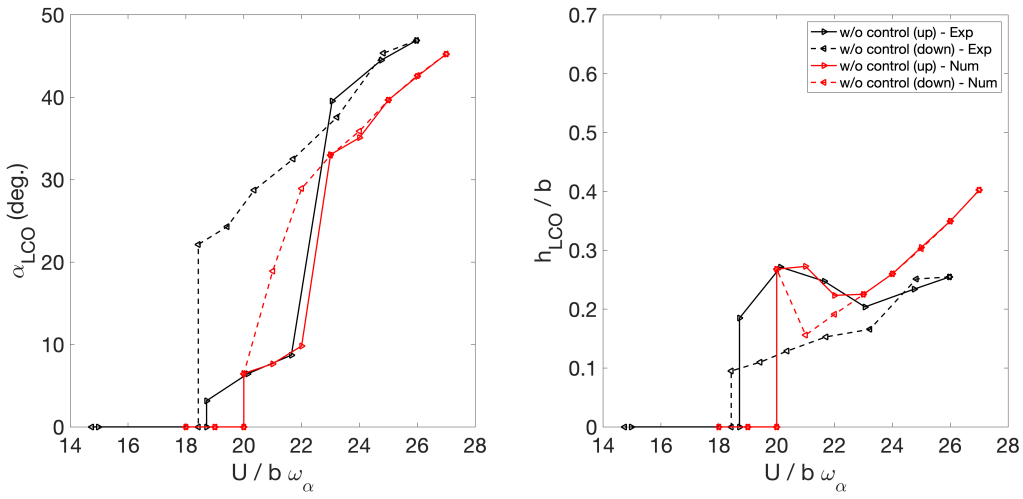

Figure 4: Post-critical behavior of a flat plate model with an elastic centre at the mid-chord: LCOs amplitude in pitch and plunge versus reduced velocity; comparison of the numerical model (red) with the experiments (black)

flutter regime. Up to $\frac{U}{U_c} \simeq 1.5$, no bifurcation to stall flutter regime was observed. As a consequence, the system remains on a coupled-mode flutter branch, with LCO amplitudes in plunge increasing strongly with the reduced velocity. A unique configuration, with both the NLTVA in plunge and NLTVA in pitch operating, has been tested. Results show that critical velocity is well repelled (an increase of almost 25%), but even with the presence of NLTVA in pitch, a switch to the stall flutter regime was observed for $\frac{U}{U_c} \simeq 1.3$, along with a strong hysteretic behavior.

Numerical results, obtained using the analytical pitch-plunge-absorbers model and the parameters of table 4 are also reported in figure 5 (bottom). As observed in experiments the TMD in plunge delays the critical velocity but the system remains in the coupled mode flutter branch before switching to the stall flutter regime with amplitude slightly lower in both pitch and plunge. Results obtained with the NLTVA in plunge are very close to the one obtained with the TDM. Regarding the NLTVA in pitch, numerical prediction does not match the one obtained in wind tunnel. Numerically this configuration delay the onset of critical velocity of almost 20% then the system immediately branches to the stall flutter regime, with amplitude slightly lower than the one observed without control. One also observed a strong hysteretic behavior decreasing the velocity from the stall flutter branch and the system still exhibit LCOs at reduced velocity 10% lower that the critical reduced velocity. With both the NLTVA in plunge and NLTVA in pitch the critical velocity is well repelled numerically (an increase of almost 30%). However, as observed in wind tunnel, a switch to the stall flutter regime is observed along with a strong hysteretic behavior. One can also notice that unlike the experiments this configuration does not mitigate the LCO in plunge in the stall flutter regime.

5 CONCLUSION

A nonlinear aeroelastic section model has been derived to compute a two branches post-critical flutter scenario observed in wind tunnel for a flat plate section model. This post-critical flutter scenario exhibits a first coupled-mode flutter branch with low amplitude in pitch and moderate amplitude in plunge, followed by a stall flutter branch with high amplitude in pitch and low amplitude in plunge. The analytical model combines a classical 2dof pitch-plunge formulation

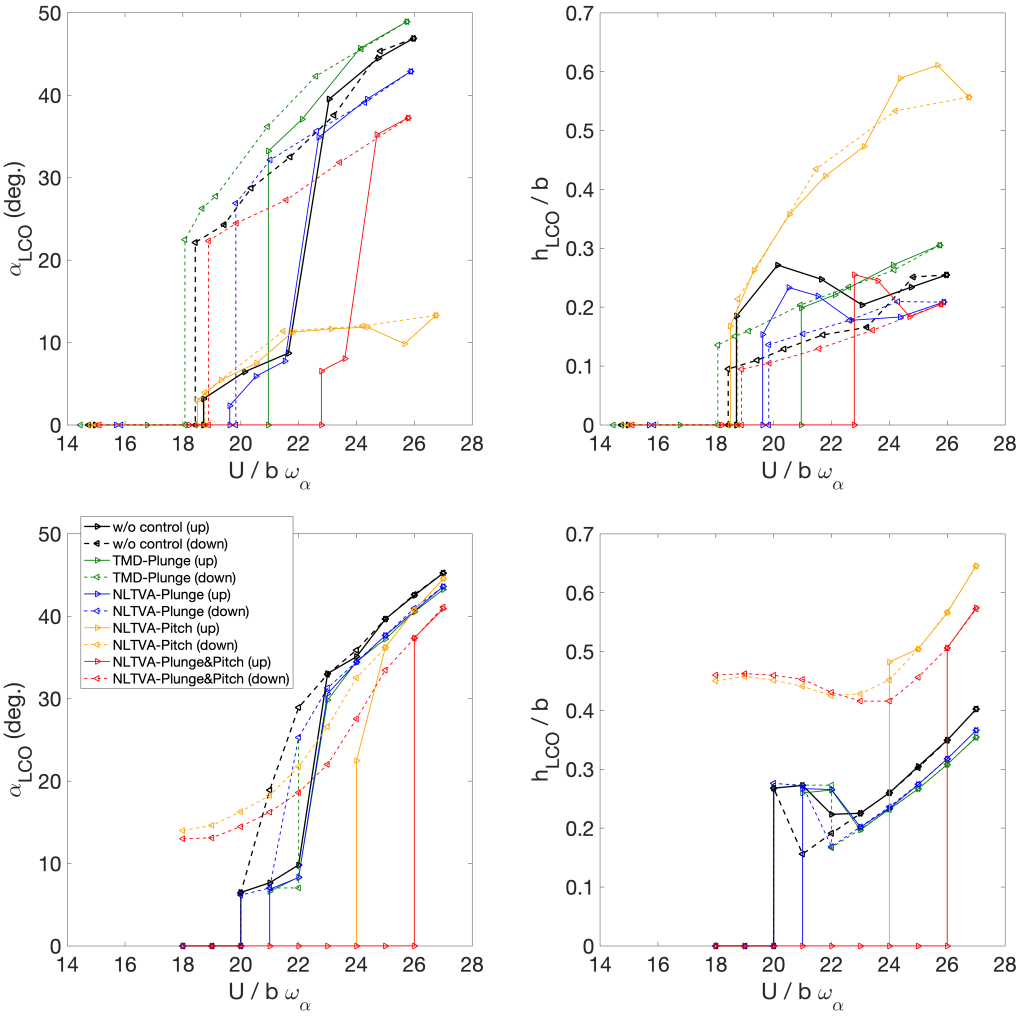

Figure 5: Influence of TMD in plunge, NLTVA in plunge, NLTVA in pitch and NLTVA in both plunge and pitch, on the post-critical behavior of a flat plate model with an elastic centre at the mid-chord; experimental results (up) and numerical predictions (bottom)

for the structurally coupled equations of motions along with a nonlinear unsteady aerodynamic formulation for both the lift and moment, based upon the ONERA semi-empirical dynamic stall model [12]. Parameters of the dynamic stall model have been validated thanks to a static and dynamic loop database obtained previously for a flat plate section model of the same thickness-to-chord ratio, in the same wind tunnel and for the same range of Reynolds number. Numerical results are in good agreement with the experiment and the two branches post-critical flutter scenario is satisfactorily reproduced. An extended version of the mathematical model, including the impact of nonlinear vibration absorbers in both pitch and plunge has then been used to play four different control configurations tested in wind tunnel: a linear TMD in plunge, a NLTVA in plunge, a NLTVA in pitch and NLTVAs in both plunge and pitch. Using linear or non linear vibrations absorbers in plunge, qualitative agreements are found. Adding non linear absorbers in pitch numerical prediction doesn't match the one obtained in wind tunnel. In was found experimentally that the NLTVA in pitch has no impact on flutter velocity and greatly delays the switch to the stall flutter regime. Numerically, one only observes an important delay of the onset of critical velocity with a direct branch to the stall flutter regime. The absorber damping ratio that have been used could be responsible for the differences observed between

numerical and experimental results. It was indeed difficult to properly identify the damping ratio of the absorber in pitch used in wind tunnel. Anyway, this study confirms that a combination of absorbers in both pitch and plunge is the best tested solution to delay the critical velocity. Further numerical investigations are ongoing in order to clarify that point, optimize the absorber tuning and find the best control strategy to repel the critical velocity and reduce the postcritical LCOs.

6 ACKNOWLEDGEMENTS

Experimental control studies have been carried out by Arnaud Malher thanks to the grant DYSACCI from Direction Générale de l'Armement (DGA). Alexandre Pecheux acknowledges his financial support for his PhD from the Agence Innovation Défense (AID).

7 REFERENCES

[1] Bisplinghoff, R. and Ashley, H. (1962). *Principles of Aeroelasticity*. John Wiley, New York.

[2] Lee, B., Price, S., and Wong, Y. (1999). Nonlinear aeroelastic analysis of airfoils: bifurcation and chaos. *Progress in aerospace sciences*, 35(3), 205–334.

[3] Dowell, E. H. (2015). Nonlinear aeroelasticity. In *A Modern Course in Aeroelasticity*. Springer, pp. 487–529.

[4] Dimitriadis, G. (2017). *Introduction to Nonlinear Aeroelasticity*. John Wiley & Sons.

[5] Amandolese, X., Michelin, S., and Choquel, M. (2013). Low speed flutter and limit cycle oscillations of a two-degree-of-freedom flat plate in a wind tunnel. *Journal of Fluids and Structures*, 43, 244–255.

[6] Amandolese, X. (2016). Low speed flutter and post-critical behaviour of flat plate and naca0018 section models in a wind tunnel. In *Proceedings of the ISFA 2016 Symposium*.

[7] Lee, Y. S., Kerschen, G., McFarland, D. M., et al. (2007). Suppressing aeroelastic instability using broadband passive targeted energy transfers, part 2: experiments. *AIAA journal*, 45(10), 2391–2400.

[8] Lee, Y., Vakakis, A., Bergman, L., et al. (2007). Suppression aeroelastic instability using broadband passive targeted energy transfers, part 1: Theory. *AIAA journal*, 45(3), 693–711.

[9] Habib, G. and Kerschen, G. (2016). Passive flutter suppression using a nonlinear tuned vibration absorber. In *Nonlinear Dynamics, Volume 1*. Springer, pp. 133–144.

[10] Malher, A., Touzé, C., Doaré, O., et al. (2016). Passive control of airfoil flutter using a nonlinear tuned vibration absorber. In *11th International Conference on Flow-induced vibrations, FIV2016*.

[11] Malher, A., Amandolese, X., Touzé, C., et al. (2017). Flutter suppression using a magnetic vibration absorber. In *7th European and African Conference on Wind Engineering, EACWE 2017*.

[12] Tran, C. and Petot, D. (1980). Semi-empirical model for the dynamic stall of airfoils in view of the application to the calculation of responses of a helicopter blade in forward flight. *Vertica*, 5(1), 35–53.

[13] Benacchio, S., Malher, A., Boisson, J., et al. (2016). Design of a magnetic vibration absorber with tunable stiffnesses. *Nonlinear Dynamics*, 85(2), 893–911.

[14] Petot, D. (1989). Modélisation du décrochage dynamique par équations différentielles. *La Recherche Aérospatiale*, (5), 59–72.

[15] Beddoes, T. (1983). Representation of airfoil behaviour. *Vertica*, 7(2), 183–197.

COPYRIGHT STATEMENT